






# Ultrafast renormalization of the magnetic continuum in the proximal Kitaev quantum spin liquid $\text{H}_3\text{LiIr}_2\text{O}_6$ by tr-RIXS [Invited]

JUNGHO KIM,<sup>1</sup> TAE-KYU CHOI,<sup>2</sup>  EDWARD MERCER,<sup>3,4</sup> LIAM T. SCHMIDT,<sup>3,4</sup> JAEKU PARK,<sup>2</sup> SANG-YOUN PARK,<sup>2</sup> DOGEUN JANG,<sup>2</sup>  SEO HYOUNG CHANG,<sup>5</sup> AYMAN SAID,<sup>1</sup> SAE HWAN CHUN,<sup>2</sup> KYEONG JUN LEE,<sup>5</sup> SANG WOOK LEE,<sup>6</sup> HYUNJEONG JEONG,<sup>6</sup> HYEONHUI JEONG,<sup>6</sup> CHANHYEON LEE,<sup>7</sup> KWANG-YONG CHOI,<sup>7</sup> FARANAK BAHRAMI,<sup>8</sup> FAZEL TAFTI,<sup>8</sup> MARTIN CLAASSEN,<sup>9,10</sup> AND ALBERTO DE LA TORRE<sup>3,4,\*</sup> 

<sup>1</sup>Advanced Photon Source, Argonne National Laboratory, Argonne, IL, USA

<sup>2</sup>XFEL Division, Pohang Accelerator Laboratory, POSTECH, Pohang, Gyeongbuk 37673, Republic of Korea

<sup>3</sup>Department of Physics, Northeastern University, Boston, MA 02115, USA

<sup>4</sup>Quantum Materials and Sensing Institute, Northeastern University, Burlington, MA 01803, USA

<sup>5</sup>Department of Physics, Chung-Ang University, Seoul 06974, Republic of Korea

<sup>6</sup>Department of Physics, Ewha Womans University, Seoul 03760, Republic of Korea

<sup>7</sup>Department of Physics, Sungkyunkwan University, Suwon 16419, Republic of Korea

<sup>8</sup>Department of Physics, Boston College, Chestnut Hill, MA 02467, USA

<sup>9</sup>Department of Physics and Astronomy, University of Pennsylvania, Philadelphia, PA 19104, USA

<sup>10</sup>Center for Computational Quantum Physics, Flatiron Institute, 162 5th Ave, New York, NY 10010, USA

\*a.delatorreduran@northeastern.edu

**Abstract:** We present the first circularly polarized non-resonant pump time-resolved resonant inelastic X-ray scattering (tr-RIXS) experiment in  $\text{H}_3\text{LiIr}_2\text{O}_6$ , an iridium-based Kitaev system. Our calculations and experimental results are consistent with the modification of the low-energy magnetic excitations in  $\text{H}_3\text{LiIr}_2\text{O}_6$  only during illumination by the laser pulse. We discuss these results in a cooperative framework between the Floquet engineering of the exchange interactions and the dynamic renormalization of electron-electron correlations. However, the penetration length mismatch between the X-ray probe and laser pump and the intrinsic complexity of Kitaev magnets prevents us from unequivocally extracting towards which ground state  $\text{H}_3\text{LiIr}_2\text{O}_6$  is driven. We outline possible solutions to these challenges for light-driven stabilization and observation of the Kitaev quantum spin liquid limit by RIXS.

Published by Optica Publishing Group under the terms of the [Creative Commons Attribution 4.0 License](https://creativecommons.org/licenses/by/4.0/). Further distribution of this work must maintain attribution to the author(s) and the published article's title, journal citation, and DOI.

## 1. Introduction

The development of scalable topological quantum computing promises to address a major challenge in the field: the loss of quantum information due to thermal noise and decoherence [1,2]. In a topological qubit, quantum information is encoded in the topological protected properties of Majorana zero modes, fractionalized excitations with non-Abelian statistics, making them robust to local distortions and perturbations [3,4]. While experimental demonstration and control of Majorana fermions in superconductor-semiconductor nanowire devices remains inconclusive [5], the Kitaev Quantum Spin Liquid (QSL) systems might offer an alternative solid-state platform to access anyon statistics [6,7]. QSLs refer to exactly solvable quantum

spin liquid states [8,9] emerging from a set of highly-frustrated spin-1/2 transition metal ions on a two-dimensional honeycomb lattice interacting via bond-directional Ising-like interactions that give rise to fractionalized Majorana and gauge flux excitations [6]. Moreover, the KQSL was predicted to be realizable in strong spin-orbit coupling quantum materials hosting honeycomb planes with edge-sharing transition metal-ligand octahedra [10,11], opening a new avenue for topological quantum computing.

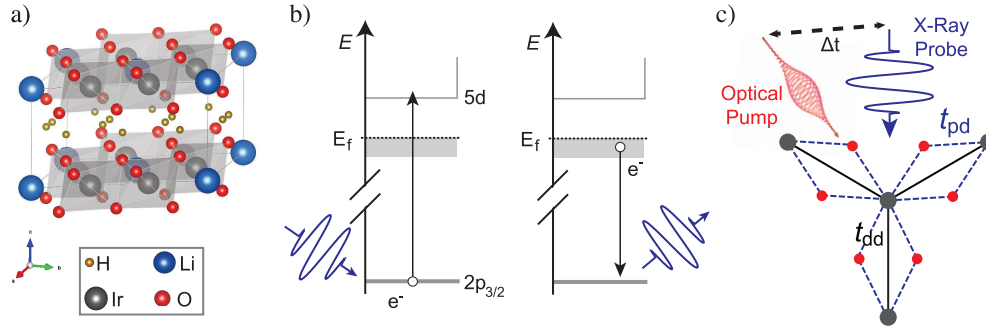


**Fig. 1.** Tr-Floquet-RIXS in  $\text{H}_3\text{LiIr}_2\text{O}_6$ . a) Crystal structure of  $\text{H}_3\text{LiIr}_2\text{O}_6$ , illustrating the layered arrangement of the  $\text{IrO}_6$  octahedra (gray) and interlayer  $\text{H}$  ions (gold). b) Schematic of the electronic transitions involved in the RIXS process at the Ir  $L_3$  edge. Left: A resonant x-ray excites a  $2p_{3/2}$  core electron into an unoccupied  $5d$  state above the Fermi level, creating an electron-hole pair. Right: An electron below the Fermi level decays, annihilating the core-hole, emitting a photon, and returning to the original state. c) Schematic of the tr-Floquet-RIXS approach. The circularly polarized optical pump will induce non-equilibrium dynamics, and then, after a delay ( $\Delta t$ ), an x-ray probe is used to measure the system's response via RIXS and provide insight into excited-state dynamics and interactions within the  $\text{IrO}_6$  lattice.

However, most Kitaev candidate materials display magnetically ordered ground states [12]. Additional efforts to access the Kitaev limit via external fields, such as hydrostatic pressure and strong magnetic fields [13,14] or atomic substitution [15] have been prevented by the presence of a dimerization instability in the phase diagram of Kitaev magnets and the resilience of the long-range ordered magnetic state to external tuning fields [16].  $\text{H}_3\text{LiIr}_2\text{O}_6$  (Fig. 1(a)) stands as the singular known candidate that lacks long-range order down to low temperature and exhibits all the characteristic properties associated with quantum spin liquids [17–19]. Moreover, a recent momentum, energy, and temperature dependent Resonant Inelastic X-ray Scattering (RIXS) experiment at the Ir  $L_3$  absorption-edge [20] uncovered a broad continuum of magnetic excitations centered at  $E = 25$  meV with a high energy tail extending up to  $E = 170$  meV. This observation aligns with expectations for dominant ferromagnetic Kitaev interactions,  $|K| = 25$  meV. Similarly, a continuum of magnetic excitations were observed in inelastic neutron scattering measurement in  $\text{D}_3\text{IrLi}_2\text{O}_6$  [21]. However, the lack of translation symmetry of the magnetic continuum [20,22], the divergence of the specific heat at low temperatures, the existence of non-vanishing contributions to the NMR response [17] and the time-field scaling of the longitudinal field  $\mu\text{SR}$  [23] indicate the presence of low energy excitations in  $\text{H}_3\text{LiIr}_2\text{O}_6$  due to a departure from the pure KQSL limit. As such,  $\text{H}_3\text{LiIr}_2\text{O}_6$  has been interpreted as displaying a dynamically fluctuating ground state near bond-disordered versions of the KQSL [24]. Thus, the experimental realization of the KQSL remains elusive despite concerted synthesis and pressure engineering efforts.

An emerging approach to controlling quantum materials is to deploy ultrafast light-matter interaction to access phases of matter unstable in equilibrium [25]. In this context, proposals to modify exchange interactions in magnetic Mott insulators by dressing the electron hopping

by the oscillating laser electric field in the minimal coupling limit (Floquet description) have attracted much attention [26–30]. For comprehensive reviews of Floquet engineering of quantum materials, we refer the reader to Refs. [25,31] and references therein. In this regime, if absorption resonances are avoided the charge subsystem remains unchanged, while a non-thermal regime can be reached in which local moments interact via renormalized magnetic interactions. When deployed to Kitaev magnets, Floquet engineering with a circularly polarized laser pulse has been numerically shown to enable the controllable and independent tuning of magnetic exchange interactions beyond Heisenberg exchange [32–34] (Fig. 1(b)). Similarly, electron-electron correlations, namely Hubbard  $U$ , have been predicted [35] and experimentally shown [36,37] to be controllable via strong laser pulses. Thus, ultrafast light-matter interaction emerges as a unique tuning knob to traverse the complex phase diagram of Kitaev magnets [38] as a function of pump laser frequency and fluence towards the transient KQSL limit.

Here, we employ time-resolved RIXS (tr-RIXS) (Fig. 1(c)) at the Pohang Accelerator Laboratory X-ray Free-Electron Laser (PAL-XFEL) facility in combination with circularly polarized strong 1900 nm laser pulses ( $F = 97 \text{ mJ/cm}^2$ ) to study the Floquet Engineering of magnetic exchange interactions in  $\text{H}_3\text{LiIr}_2\text{O}_6$ . tr-RIXS is a uniquely suited technique to access transient changes to the magnetic spectrum of quantum materials with sub-ps resolution. This study builds directly on recent tr-RIXS measurements at the Ir  $L_3$ -edge on related iridate compounds [5], including  $\text{Sr}_2\text{IrO}_4$  [39],  $\text{Sr}_3\text{Ir}_2\text{O}_7$  [40], and  $\alpha\text{-Li}_2\text{IrO}_3$  [41]. These pioneering efforts established the feasibility of probing ultrafast magnetic and electronic excitations in 5d Mott insulators using XFEL-based hard x-ray RIXS. In contrast to previous work, which typically employed linearly polarized resonant pump pulses and focused on layered iridates with long-range magnetic order, our study investigates  $\text{H}_3\text{LiIr}_2\text{O}_6$ —a bond-disordered, proximate Kitaev spin liquid—under circularly polarized, non-resonant pumping. This unique combination allows us to explore transient dynamics during illumination in a system lacking long-range order. Our data, emerging from the first non-resonant excitation tr-RIXS experiment on a Kitaev magnet, are suggestive of an increase in coherence of the magnetic excitations only during pump illumination. On the other hand, calculations of the variation of the magnetic exchange interactions within the Floquet description as a function of laser pump frequency and fluence predict an evolution of  $\text{H}_3\text{LiIr}_2\text{O}_6$  toward the KQSL limit at the sample surface but less than 1% change when averaged over the probed sample volume. We discuss this dichotomy within a cooperative effect of Floquet engineering and dynamic renormalization of electron-electron interactions. Our data and calculations exemplify the intrinsic complexity of Kitaev magnets and of hard X-ray probe-laser pump experiments. We conclude with a discussion of how this pioneering experiment, demonstrating transient changes to the magnetic excitations of a topical quantum material, opens new pathways to transiently accessing control over the KQSL phase.

## 2. Materials and methods

### 2.1. Sample growth and characterization

The samples are from the same batch as in Ref. [20]. Precursor single crystals of  $\alpha\text{-Li}_2\text{IrO}_3$  were grown as described elsewhere [42].  $40 \times 40 \mu\text{m}$  single crystals of  $\text{H}_3\text{LiIr}_2\text{O}_6$  were grown via a topotactic exchange by placing  $\alpha\text{-Li}_2\text{IrO}_3$  inside an autoclave filled with sulfuric acid for 48 hours [22]. The replacement of the inter-honeycomb layer Li with H leads to a modification of the intra-layer Ir-O-Ir bond angles and of the superexchange pathways. The proximal KQSL state was characterized by powder x-ray diffraction, specific heat, magnetization measurements [15], and static RIXS. Before the tr-RIXS experiment, samples were aligned with by synchrotron XRD at the IVU - Undulator Beamline of the Canadian Light Source (CLS). For the tr-RIXS experiment, the scattering plane was set along  $[HOL]$ .

## 2.2. *tr*-RIXS setup at the PAL-XFEL

Despite extensive efforts to discover materials exhibiting quantum spin liquid behavior under equilibrium conditions, such discoveries have remained inconclusive. The process of renormalizing magnetic exchange parameters through photo-assisted virtual hopping pathways offers a promising opportunity to identify topological excitations within the quantum spin liquid. In this regard, the use of *tr*-RIXS experimental setup at the XFEL facility emerges as the primary spectroscopic tool for monitoring the emergence of non-equilibrium quantum phases, with particular attention to intensity modulations as a function of momentum, which provide critical insights into these phenomena [39–41,43–45].

The *tr*-RIXS experiment was conducted at the X-ray Scattering and Spectroscopy (XSS) hutch of the PAL-XFEL [46]. Self-seeded hard x-ray pulses were generated with the electron bunch charge of 170 pC and the undulator  $K$  parameter of 1.87 with a period of 28 mm [47]. A narrowband seed pulse was filtered after eight 5 m-long undulators by forward Bragg diffraction (FBD) of the [224] peak through a 100  $\mu\text{m}$ -thick diamond [100] crystal [48]. The seed pulse was then directed by a bandpass filter with a delay of tens of femtoseconds, and overlapped in time with the detoured electron bunch by a magnetic chicane to amplify the narrow seed intensity in the following undulators [49]. The incident XFEL beam was assessed by diagnostic tools placed along the beamline from upstream to downstream [50]. To calibrate the incident photon energy, we measured the x-ray absorption spectrum of  $\text{IrO}_2$  powder sample in total fluorescence yield at room temperature, as shown in Fig. 2 (a).

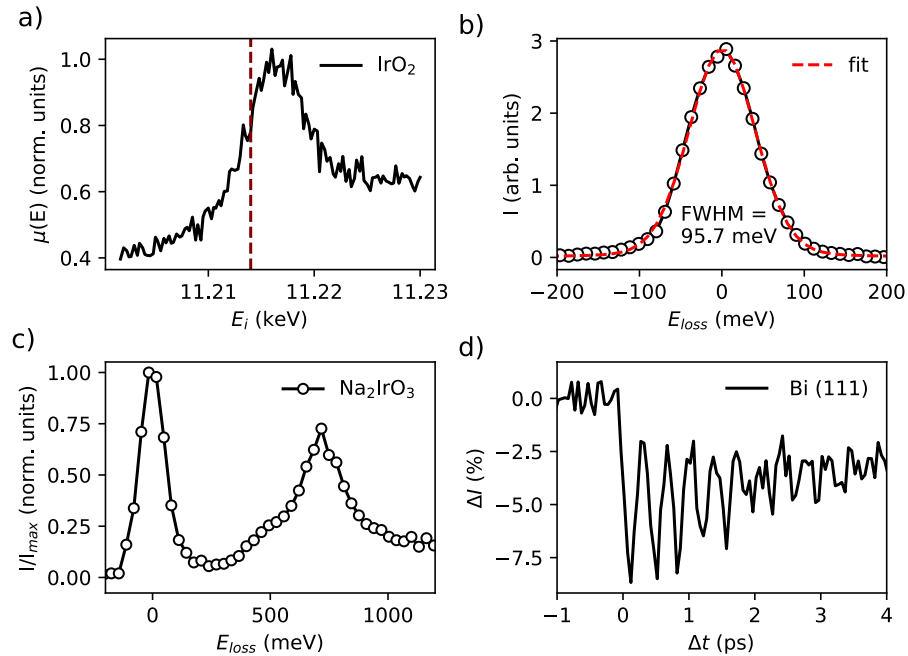


**Fig. 2.** Characterization of the *tr*-RIXS experimental setup at the PAL-XFEL. a) X-ray absorption spectrum of  $\text{IrO}_2$  powder sample measured in total fluorescence yield at room temperature. The vertical dashed line indicates the main  $\text{Ir } L_3$  resonance at  $E_i = 11214 \text{ eV}$ . b) Elastic scattering from a Scotch tape (circular markers) and fit to a Pseudo-Voigt profile (red dashed line) with a  $\text{FWHM} = 95.7 \text{ meV}$ . c) Room temperature RIXS spectrum of  $\text{Na}_2\text{IrO}_3$  measured at  $\Gamma$  for 15 min. d) Transient light-induced modulation of the  $\text{Bi } (111)$  Bragg peak intensity after arrival of a 1900 nm laser pulse with  $F = 97 \text{ mJ cm}^{-2}$ .

For the RIXS setup, a spherically bent analyzer (diameter = 100 mm, radius of curvature = 1000 mm) with Si(844) diced crystals ( $2 \times 2 \text{ mm}^2$ ) was positioned at  $2\theta = 90^\circ$ . A two-dimensional (2D) JUNGFRU detector (pixel size =  $75 \text{ }\mu\text{m}$ ) was aligned to the Rowland circle for the Bragg reflection of  $E_i = 11214 \text{ eV}$  ( $\theta_B = 86^\circ$ ) in the vertical diffraction plane. The detector's active area was shielded with lead tape except for an opening to the crystal analyzer to minimize background. The Bragg angle of the Si(844) crystal analyzer was slightly increased such that the elastic peak is close to the highest energy within the 1.6 eV energy dispersion window of the Si(844) dice. The output from the JUNGFRU was converted from pixel to energy by applying a calibration factor of  $epp = 31.87 \text{ meV pixel}^{-1}$ . An avalanche photodiode (APD) was installed on the same side of the Si(844) crystal analyzer to monitor x-ray fluorescence from the sample. A helium-flowing environment was made along the x-ray flight paths. The self-seeded pulses at a repetition rate of 60 Hz were then focused to a spot size of  $20 \text{ }\mu\text{m}$  in full width at half maximum (FWHM) at the sample position by a set of beryllium compound refractive lenses (CRLs). Unless specified, the average x-ray pulse energy was  $15 \text{ }\mu\text{J}$  after the CRLs. To calibrate the energy resolution of the spectrometer, we measured elastic scattering signal from a Scotch tape while tuning a double-crystal monochromator (DCM) from Si(111) to Si(333) Bragg diffraction with the electron bunch energy and the FBD of diamond [100] crystal kept at their optimal condition for the Ir  $L_3$  edge,  $E_i = 11214 \text{ eV}$ . Figure 2 (b) shows the reference elastic signal for the spectrometer with an optimal resolution of  $\Delta E = 95.7 \text{ meV}$ , extracted from a fit to a Pseudo-Voigt line shape. The sample environment was set by a nitrogen-flow cryostat with a base temperature of  $T = 100 \text{ K}$ . Figure 2 (c) shows an energy loss spectrum ( $E_{\text{loss}} = E_i - E_f$ ) at  $\Gamma$  for a  $\text{Na}_2\text{IrO}_3$  single crystal with optimal resolution measured at room temperature. To prevent radiation damage on the sample at resonance, the x-ray was defocused to a spot size of  $146 \text{ }\mu\text{m}$ , which degraded the resolution to  $\Delta E \approx 120 \text{ meV}$ .

Near-infrared (NIR) laser pulses (100 fs in FWHM) were synchronized to the half-repetition rate of the XFEL pulses, i.e., 30 Hz, and propagated at the incident angle of  $10^\circ$  with respect to the XFEL. Data acquisition by the JUNGFRU detector was synchronized to the XFEL repetition rate and tagged (laser on, laser off) for data analysis. The laser was focused to a spot size of  $340 \text{ }\mu\text{m}$  in FWHM at the sample interaction point, and its fluence was set to  $97 \text{ mJ cm}^{-2}$ , corresponding to a peak electric field  $E = 5.4 \text{ GV/m}$ . For this experiment, the pump laser was set at 1900 nm, such that the drive photon energy is proximal but non-resonant with the Ir intra- $t_{2g}$  excitations to minimize heating effects [20]. A spatiotemporal overlap between the x-ray and 1900 nm laser pulses was determined by tracking the transient modulation of a Bi(111) Bragg peak intensity [51]. The decay at  $\Delta t = 0 \text{ ps}$ , when optical pump and x-ray probe arrive simultaneously at the sample, and subsequent oscillations of the Bragg peak intensity due to photoexcited phonon dynamics observed in Fig. 2(d) confirm the stable arrival time and synchronization of the pair of XFEL and laser pulses without the need for timing-jitter corrections. The overall time resolution, i.e., instrument response function, of the tr-RIXS setup was determined to be 167 fs in FWHM.

### 3. Results and discussion

The main experimental results of our work are summarized in Fig. 3. Each data set is the average of between 5 and 10 independent measurements, in which successive pairs of pump-on/pump-off measurements were collected for 12 min each. Error bars at each energy are calculated from the mean standard deviation over this set of measurements. In Fig. 3 (a)-(c), we show the RIXS spectra at grazing incidence ( $\alpha = 0.5^\circ$  or  $\alpha = 0.2^\circ$ ) from  $\text{H}_3\text{LiIr}_2\text{O}_6$  with and without the incident 1900 nm circularly polarized laser pulse of  $F = 97 \text{ mJ/cm}^2$  at three different time delays: a),  $\Delta t = -1 \text{ ps}$ , b),  $\Delta t = 0 \text{ ps}$ , and c),  $\Delta t = 5 \text{ ps}$ . To evaluate the effect of the circular pump at 1900 nm on the RIXS spectrum of  $\text{H}_3\text{LiIr}_2\text{O}_6$ , we plot the relative change,  $\Delta I/I = (I_{\text{on}} - I_{\text{off}})/(I_{\text{on}} + I_{\text{off}})$ , in Fig. 3 (d)-(f). The lack of statistically significant changes in the elastic RIXS response at earlier time delays,  $\Delta t = -1 \text{ ps}$  [Fig. 3 (d)], indicates the absence of average heating effects despite



the large pump fluence. The observed  $\Delta I/I \approx 0$  at later times  $\Delta t = 5$  ps [Fig. 3 (f)], particularly in the energy range of the intra- $t_{2g}$  excitations in  $\text{H}_3\text{LiIr}_2\text{O}_6$  ( $E_{\text{loss}} \in [500, 1200]$  meV) [20], confirms the non-resonant nature of the laser excitation, and rules out a hot phononic bath, which generally thermalizes in  $\approx 10$  ps timescales [52–54], and a charge renormalization due to the creation of holon-doublon pairs in a driven Mott insulator [55,56]. On the other hand, at  $\Delta t = 0$  ps, we observe changes in the RIXS intensity above the largest mean standard deviation in the  $E_{\text{loss}} \in [50, 300]$  meV range, the tail of the broad magnetic continuum in  $\text{H}_3\text{LiIr}_2\text{O}_6$  associated with the presence of fractionalized excitations [20], that vanish at  $\Delta t = 5$  ps. We note that such fast dynamics are unusual given the insulating nature of  $\text{H}_3\text{LiIr}_2\text{O}_6$  [12] and the lack of phononic excitations in this energy loss range [19]. Thus, our data suggest that the non-resonant circularly polarized excitation in  $\text{H}_3\text{LiIr}_2\text{O}_6$  leads to photo-induced gain of coherence of the magnetic excitations in  $\text{H}_3\text{LiIr}_2\text{O}_6$ , possibly due to the transient modification of the exchange interactions and the suppression of magnetic fluctuations towards a magnetically ordered state.

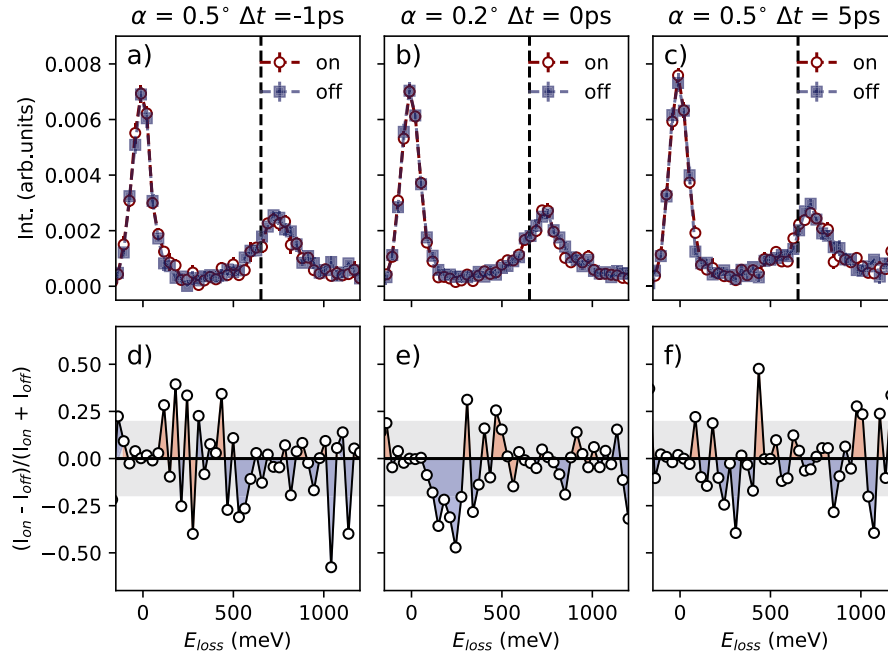


**Fig. 3.** Ultrafast modification of the magnetic excitations in  $\text{H}_3\text{LiIr}_2\text{O}_6$ . a)-c) RIXS spectrum at resonance and  $T = 100$  K with (on, red circular markers) and without (off, blue square markers) a 1900 nm laser pulse at various time delays: a),  $\Delta t = -1$  ps, the average of 5 individual scans of 12 min exposure for each condition b),  $\Delta t = 0$  ps, the average of 10 individual scans, and c),  $\Delta t = 5$  ps, the average of 4 individual scans. The vertical dashed line signal encodes the energy of the laser pump.  $\alpha$  is the angle of incidence of the x-ray. d)-e) Relative change of the RIXS spectrum due to the laser pulse at d),  $\Delta t = -1$  ps, e),  $\Delta t = 0$  ps, and, f),  $\Delta t = 5$  ps scans. The gray bar illustrates the mean standard deviation. Red and blue shading indicates increased or decreased intensity due to the laser excitation.

Our tr-RIXS data is thus reminiscent of predictions of Floquet engineering of magnetic excitations in Kitaev spin liquids [32–34]. To capture the pump-induced modification of Kitaev and Heisenberg exchange couplings only during the pump illumination, we study a minimal model of two neighboring Ir ions coupled via ligand-mediated electron tunneling processes. A single hole resides on average in the  $t_{2g}$  orbital manifold per Ir site, which splits into  $j_{\text{eff}} = 1/2$  and  $j_{\text{eff}} = 3/2$  states via strong spin-orbit coupling  $\lambda$ . In the large cubic crystal field limit, a

combination of strong local Coulomb ( $U$ ) and Hund's ( $J_H$ ) interactions opens a gap for charge excitations. The Kanamori-type Hamiltonian  $H_U$  is given by

$$\begin{aligned} \hat{H}_0 = & U \sum_{i\alpha} \hat{n}_{i\alpha\uparrow} \hat{n}_{i\alpha\downarrow} + \sum_{i\sigma\sigma', \alpha < \beta} (U' - \delta_{\sigma\sigma'} J_H) \hat{n}_{i\alpha\sigma'} \hat{n}_{i\beta\sigma} \\ & + J_H \sum_{i, \alpha \neq \beta} \left( \hat{c}_{i\alpha\uparrow}^\dagger \hat{c}_{i\alpha\downarrow}^\dagger \hat{c}_{i\beta\downarrow} \hat{c}_{i\beta\uparrow} - \hat{c}_{i\alpha\uparrow}^\dagger \hat{c}_{i\alpha\downarrow} \hat{c}_{i\beta\downarrow}^\dagger \hat{c}_{i\beta\uparrow} \right) + \frac{\lambda}{2} \sum_i \mathbf{c}_i^\dagger (\mathbf{L} \cdot \mathbf{S}) \mathbf{c}_i \end{aligned} \quad (1)$$

with  $i$  summing over the Ir sites, and  $\alpha, \beta$  indexing the  $t_{2g}$  orbitals of Ir. We assume  $C_3$  rotation symmetry, which neglects a weak additional crystal field splitting.

Hopping between Ir sites is modeled by four Slater-Koster parameters  $t_{xz,xz}, t_{xz,yz}, t_{xy,xy}$  and  $t_{xz,xy}$ . Electrons are coupled to light via the Peierls substitution  $\hat{c}_{i\alpha}^\dagger \hat{c}_{j\alpha'} \rightarrow e^{i \frac{e}{\hbar} \mathbf{r}_{ij} \cdot \mathbf{A}(t)} \hat{c}_{i\alpha}^\dagger \hat{c}_{j\alpha'}$ , where  $\mathbf{r}_{ij}$  is a bond vector and  $\mathbf{A}(t) = A[\sin(\omega t), \cos(\omega t)]$  is the vector potential for a circularly polarized laser with frequency  $\omega$ . For a periodic drive, this defines a (dimensionless) Floquet parameter  $\mathbf{r}_{ij} \cdot \mathbf{A}(t) = F \cos(\omega t)$  where  $F = a_0 e \mathcal{E} / (\hbar \omega)$  is defined via the peak electric field strength  $\mathcal{E}$  and  $a_0 = 3.1 \text{ \AA}$ , the interatomic Ir-Ir distance.  $e$  the electron charge. The hopping Hamiltonian between two sites  $i$  and  $j$  along a  $z$  bond then reads

$$\hat{H}'_{ij}(t) = \sum_{\sigma} e^{iF \cos(\omega t)} \begin{bmatrix} \hat{c}_{id_{xz}\sigma}^\dagger & \hat{c}_{id_{yz}\sigma}^\dagger & \hat{c}_{id_{xy}\sigma}^\dagger \end{bmatrix} \cdot \begin{bmatrix} t_{xz,xz} & t_{xz,yz} & t_{xz,xy} \\ t_{xz,yz} & t_{xz,xz} & t_{xz,xy} \\ t_{xz,xy} & t_{xz,xy} & t_{xy,xy} \end{bmatrix} \cdot \begin{bmatrix} \hat{c}_{jd_{xz}\sigma}^\dagger & \hat{c}_{jd_{yz}\sigma}^\dagger & \hat{c}_{jd_{xy}\sigma}^\dagger \end{bmatrix} \quad (2)$$

following the model discussed in Ref. [38,57,58].

If the pump field with frequency  $\omega$  is off-resonant from  $d-d$  excitations, charge excitations remain largely suppressed, provided the pulse duration is sufficiently short. In this case, Floquet modifications of spin exchange processes can be readily computed by simultaneously integrating out charge excitations (two-hole Ir states) and photon absorption processes via a Schrieffer-Wolff transformation [32–34]. The resulting spin Hamiltonian for a  $\gamma$ -direction bond takes the form

$$\hat{H}_{ij}^{(\gamma)} = \sum_{\langle ij \rangle_{\gamma}, \alpha\beta(\gamma)} J \hat{\mathbf{S}}_i \cdot \hat{\mathbf{S}}_j + K \hat{S}_i^\gamma \hat{S}_j^\gamma + \Gamma (\hat{S}_i^\alpha \hat{S}_j^\beta + \hat{S}_i^\beta \hat{S}_j^\alpha) \quad (3)$$

with Kitaev  $K$ , Heisenberg  $J$  and off-diagonal interactions  $\Gamma$  interactions. We neglect weak anisotropic interactions  $\Gamma'$  of the form  $\hat{S}_i^\alpha \hat{S}_j^\gamma$  [59]. Within our Floquet-Kitaev model, all exchange interactions become functions of the driving field amplitude  $A$  and frequency  $\omega$  ( $K(A, \omega)$ , Heisenberg  $J(A, \omega)$ ,  $\Gamma$ ). Physically, this dependence arises from effective photon-dressed exchange processes, whereby a hole virtually tunnels to a neighboring Ir site while absorbing a photon to mitigate its intermediate-state energy penalty due to another hole on the same site; the second hole can subsequently tunnel back and re-emit a photon [32–34]. Figure 4(a) shows the calculated light-induced modification of  $K(A, \omega)$ , Heisenberg  $J(A, \omega)$  with respect to the equilibrium values for  $U = 2.2 \text{ eV}$ ,  $J_H = 0.3 \text{ eV}$ ,  $\lambda = 0.540 \text{ eV}$ . Following Ref. [20], which directly encoded the role of structural disorder in the hopping Hamiltonian, we fix inter-Ir hopping values  $t_{xz,xz} = 0.050 \text{ eV}$ ,  $t_{xz,yz} = 0.440 \text{ eV}$ . The remaining hopping parameters are set to  $t_{xy,xy} = 0.08 \text{ eV}$  and  $t_{xz,xy} = 0.04 \text{ eV}$ , consistent with [57] and the expected equilibrium Kitaev exchange interaction  $\sim 30 \text{ meV}$ . The corresponding normalized Floquet Kitaev parameter ( $K_{eff} = K/[|J| + |K| + |\Gamma|]$ ) is shown in Fig. 4(b)). While across the range of Floquet parameters and pump wavelengths considered in our calculations, we observed the enhancement and suppression of the exchange interactions,  $K_{eff}$  shows a small increase for all parameters.

Our calculations predict that Floquet engineering can bring  $\text{H}_3\text{LiIr}_2\text{O}_6$  into the true Kitaev limit. However, this result is extremely sensitive to changes of  $U$  and the inter-orbital hopping

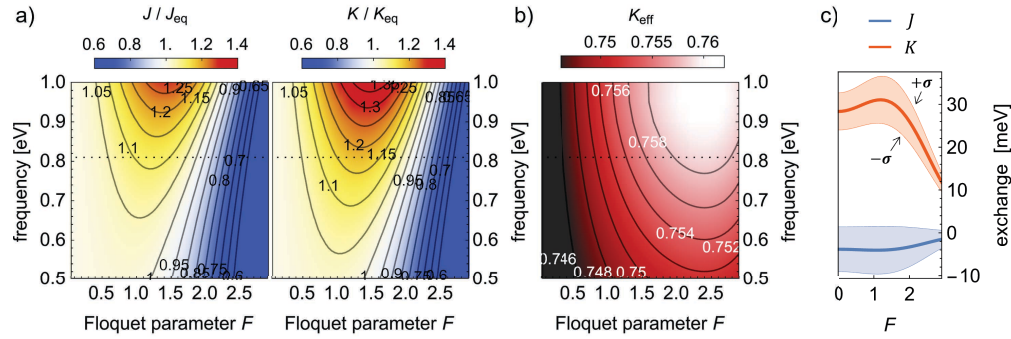


**Fig. 4.** Floquet Control of Exchange Parameters in  $\text{H}_3\text{LiIr}_2\text{O}_6$ . (a) Light-induced modification of Heisenberg ( $J(A, \omega)$ ) and Kitaev ( $K(A, \omega)$ ) exchange couplings, with respect to their values in equilibrium ( $J_{eq}, K_{eq}$ ), as a function of the Floquet parameter  $F$  and pump frequency. (b) Normalized Floquet Kitaev exchange parameter  $K_{eff} = K/[|J| + |K| + |\Gamma|]$ . Dashed line in a) and b), at  $E = 0.8$  eV, indicates the charge resonance. (c) Mean and standard deviation of the Floquet Heisenberg and Kitaev exchange parameters for  $\omega = 0.65$  eV, averaged over variations of the electronic parameters (inter-orbital hopping and Coulomb interactions).

parameters  $t_{xy,xy}$  and  $t_{xz,xy}$ . To account for this variability, in Fig. 4 c) we show the mean and standard deviation of  $J(A, \omega)$  and  $K(A, \omega)$  computed for a range of parameters  $U \in [1.9, 2.4]$  eV,  $t_{xy,xy} \in [-0.14, 0.14]$  eV and  $t_{xz,xy} \in [-0.1, 0.1]$  eV. Nonetheless, for our pump parameters,  $\omega = 0.65$  eV and fluence  $97 \text{ mJ cm}^{-2}$ , larger by two orders of magnitude than the driving field needed to generate Floquet states in graphene [60,61], gives a corresponding Floquet parameter  $F = aeE/\hbar\omega = 2.56$  comparable to that used to engineer optical nonlinearities in a 2D van der Waal material [62]. Our calculations show that for this value of  $F$ ,  $J_{eff}$  would be fully suppressed while maintaining a finite value of  $K_{eff}$  indicating a Floquet-driven transition into the KQSL limit. However, our calculations contrast with our experimental data (Fig. 3), in which the photo-induced gain of coherence of the magnetic continuum suggests a departure from the KQSL limit towards a potentially ordered magnetic state.

A second alternative explanation to the Floquet engineering of the exchange interactions is the dynamic renormalization of the Coulomb  $U$  and charge transfer energies due to the creation of delocalized states during pump illumination via multi-photon absorption processes [35–37]. Within this picture, the hopping parameters remain unaltered, but the transiently delocalized carriers screen the electron-electron interactions, leading to photo-induced modifications of the crystal field and ligand environment. This mechanism has been shown to induce changes at  $\Delta t = 0$  ps to the x-ray absorption spectroscopy spectrum in two other correlated insulators [36,37] and require weaker fluences than those needed for Floquet engineering. Under this picture, the dynamic modification of  $U$  and  $J_H$  can lead to a sudden modification of  $J$  and  $K$  and a reduction of the effective Ir spin, inducing a suppression of spectral weight in the tail of the magnetic continuum as observed in Fig. 3. Moreover, creating transiently delocalized charges could explain the slight increase in spectral weight at  $E_{loss} = 500$  meV observed in Fig. 3 (e). Nonetheless, we note that crystal field excitations in  $\text{H}_3\text{LiIr}_2\text{O}_6$  are broad and modifications of  $U$  and  $J_H$  have small to no effect on the energy of the intra- $t_{2g}$  excitations in iridates, where the dominant intra-atomic energy scale is  $\lambda$  [63].

However, the penetration depth mismatch between the pump laser and the hard X-ray probe must be taken into account. At the Ir  $L_3$ , based on the  $\text{H}_3\text{LiIr}_2\text{O}_6$  density  $\rho = 3.620 \text{ g/cm}^3$  and the Ir atomic absorption coefficient [64], we calculate a penetration depth of the hard x-ray beam in  $\text{H}_3\text{LiIr}_2\text{O}_6$  probe of approximately  $10 \mu\text{m}$ . On the other hand, based on that of  $\alpha\text{-Li}_2\text{IrO}_3$ , the absorption coefficient of  $\text{H}_3\text{LiIr}_2\text{O}_6$  at NIR wavelengths is  $\alpha \approx 300 \text{ nm}$  [65]. Figure 5(a)-b)



shows the evolution of  $E$  and  $F$ . After the first  $2\mu\text{m}$ ,  $F$  is negligible, and so are the effects of the laser electric field on the exchange interactions of  $\text{H}_3\text{LiIr}_2\text{O}_6$  (Fig. 5(c)). However, the average Floquet parameter over the sample estimated thickness ( $d = 5\mu\text{m}$ ),  $\bar{F} = 0.128$ , would lead to small changes of  $\Delta K/K_{\text{eff}} = 0.12\%$  and  $\Delta J/J_{\text{eff}} \approx -0.7\%$ . While the dependence of  $J_{\text{eff}}$  and  $K_{\text{eff}}$  on model parameters should also be considered in the low  $F$  regime, making calculating the expected changes to the exchange interactions difficult, the small effective modification of the exchange parameters should not lead to changes in the coherence or to resolvable changes in the center energy of the continuum. On the other hand, the dynamical screening of electron-electron interactions requires order of magnitude weaker fluences [36]. It is thus possible that the observed ultrafast changes to the magnetic excitations in  $\text{H}_3\text{LiIr}_2\text{O}_6$  emerge due to a cooperative interplay of Floquet engineering and dynamic renormalization of electron-electron interactions. Nonetheless, the changes observed in the low-energy magnetic continuum of  $\text{H}_3\text{LiIr}_2\text{O}_6$  during pump illumination are more modest than those reported in previous XFEL RIXS studies on Ruddlesden-Popper (RP) perovskite iridates [39,40]. However, this distinction reflects fundamental differences in the ground states: while RP iridate possesses well-defined magnon modes tied to long-range order,  $\text{H}_3\text{LiIr}_2\text{O}_6$  hosts a disordered, dynamically fluctuating magnetic state even at low temperatures. Consequently, the transient enhancement of magnetic coherence reported here may represent an initial step toward light-induced ordering in a system where no such order exists in equilibrium. This highlights the challenges and opportunities of Floquet engineering in bond-disordered quantum spin liquids. While the tr-RIXS signal observed in  $\text{H}_3\text{LiIr}_2\text{O}_6$  is relatively subtle, we emphasize that the novelty of our work lies in both the experimental platform and the system under study. Our implementation departs significantly from earlier tr-RIXS setups by employing circularly polarized, 1900 nm pulses in a non-resonant Floquet-driving regime.

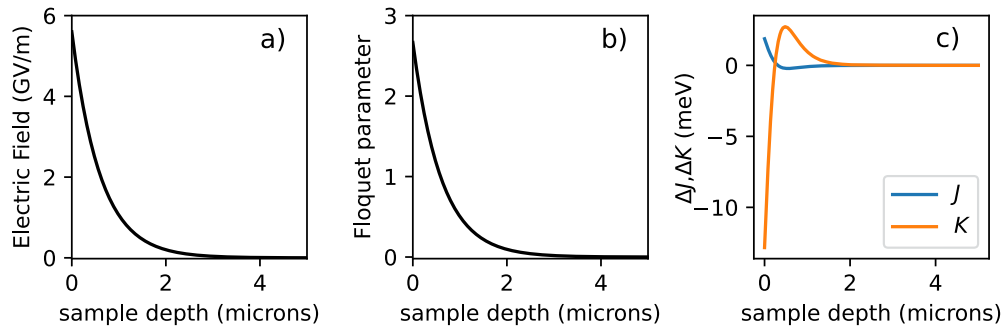


**Fig. 5.** Effects of the penetration depth mismatch. Evolution of a) the Electric field,  $E$ , b) the Floquet parameter,  $F$  and c) Floquet-induced modification of the exchange interactions,  $\Delta J = J(A, \omega) - J_{\text{eq}}$ ;  $\Delta K = K(A, \omega) - K_{\text{eq}}$  as a function of the sample depth.

#### 4. Conclusions and outlook

Altogether, our theoretical calculations and experimental results establish photo-induced effects during pump illumination as a new approach to tune the magnetic Hamiltonian of Kitaev magnets. However, the intrinsic complexity of time-resolved hard X-ray experiments in light-engineered quantum magnets, namely exchange frustration, structural disorder, decoherence, and penetration depth mismatch, hinders us from conclusively demonstrating the realization of the light-induced KQSL. To unequivocally demonstrate the light-matter engineering of long-range entangled magnetic ground states in Kitaev magnets, a systematic approach combining improved material synthesis, pump-probe-specific sample fabrication and methodology, theory, and experiment

development is needed. In the context of *Kitaev magnets for out of equilibrium*, a possible avenue is to consider other new generation iridium-based Kitaev magnets beyond  $\text{H}_3\text{LiIr}_2\text{O}_6$  [15]. Recently,  $\text{D}_3\text{LiIr}_2\text{O}_6$  [21] has emerged as an alternative since the heavier deuterium atoms will lead to fewer stacking faults in the structure than in  $\text{H}_3\text{LiIr}_2\text{O}_6$ . Alternatively, the use of exfoliated flakes or thin films of iridium-based Kitaev magnets could minimize the penetration depth mismatch between the laser pump and X-ray probe. On the other hand, pump and probe penetration depths are comparable in Kitaev materials with transition metal oxides with  $L$  edges in the soft X-ray regime. We highlight earth-abundant cobalt-based Kitaev material, such as  $\text{Na}_2\text{Co}_2\text{TeO}_6$ , as a platform for future experiments [66]. The results presented serve as stepping stone towards achieving the elusive Kitaev limit and will motivate future tr-RIXS experiments in Kitaev magnets as well as presenting the need to develop a formal theory of fractionalized excitations in Floquet KQSLs and their signatures in tr-RIXS.

**Funding.** Ministry of Science and ICT, South Korea (RS-2022-00164805); Basic Energy Sciences (DE-SC0023124, DE-SC0024494).

**Acknowledgment.** Sample characterization by XRD was performed at the Canadian Light Source, a national research facility of the University of Saskatchewan, which is supported by the Canada Foundation for Innovation (CFI), the Natural Sciences and Engineering Research Council (NSERC), the Canadian Institutes of Health Research (CIHR), the Government of Saskatchewan, and the University of Saskatchewan. Experiments at 3A beamline of PLS-II were supported in part by MIST. The use of the Advanced Photon Source at the Argonne National Laboratory was supported by the U.S. DOE Office of Science-Basic Energy Sciences, under Contract No. Contract DE-AC02-06CH11357. The authors thank all staff members of the PAL-XFEL for supporting the tr-RIXS experiment. The experiment was performed using the FXS instrument at the PAL-XFEL (Proposal No. 2024-1st-XSS-013) funded by the Ministry of Science and ICT of Korea (RS-2022-00164805). The authors thank the Global Science Experimental Data Hub Center (GSDC) at the Korea Institute of Science and Technology Information (KISTI) for providing computing resources and technical support. The work at Boston College was funded by the U.S. Department of Energy, Office of Basic Energy Sciences, Division of Physical Behavior of Materials under award number DE-SC0023124. M. C. acknowledges support from the U.S. Department of Energy, Office of Basic Energy Sciences, under Award No. DE-SC0024494. A.d.I.T. acknowledges helpful conversations with Kemp Plumb, Hui-Yuan Daniel Chen, and Greg Fiete.

**Disclosures.** The authors declare no conflicts of interest.

**Data availability.** Data underlying the results presented in this paper may be obtained from the authors upon reasonable request.

## References

1. M. Schlosshauer, "Quantum decoherence," *Phys. Rep.* **831**, 1–57 (2019).
2. M. Onizhuk and G. Galli, "Decoherence of solid-state spin qubits: a computational perspective," (2024).
3. R. S. K. Mong, D. J. Clarke, J. Alicea, *et al.*, "Universal topological quantum computation from a superconductor-abelian quantum Hall heterostructure," *Phys. Rev. X* **4**(1), 011036 (2014).
4. C. Easttom, *Topological Quantum Computing* (Springer Nature Switzerland, Cham, 2024, pp.113–123).
5. Z. Cao, S. Chen, G. Zhang, *et al.*, "Recent progress on majorana in semiconductor-superconductor heterostructures—engineering and detection," *Sci. China Phys. Mech. Astron.* **66**(6), 267003 (2023).
6. A. Kitaev, "Anyons in an exactly solved model and beyond," *Ann. Phys.* **321**(1), 2–111 (2006).
7. A. Kitaev and C. Laumann, "Topological phases and quantum computation," (2009).
8. L. Savary and L. Balents, "Quantum spin liquids: a review," *Rep. Prog. Phys.* **80**(1), 016502 (2017).
9. C. Broholm, R. J. Cava, S. A. Kivelson, *et al.*, "Quantum spin liquids," *Science* **367**(6475), eaay0668 (2020).
10. J. G. Rau, E. K.-H. Lee, and H.-Y. Kee, "Spin-orbit physics giving rise to novel phases in correlated systems: iridates and related materials," *Annu. Rev. Condens. Matter Phys.* **7**(1), 195–221 (2016).
11. G. Jackeli and G. Khaliullin, "Mott insulators in the strong spin-orbit coupling limit: from Heisenberg to a quantum compass and Kitaev models," *Phys. Rev. Lett.* **102**(1), 017205 (2009).
12. H. Takagi, T. Takayama, G. Jackeli, *et al.*, "Concept and realization of Kitaev quantum spin liquids," *Nat. Rev. Phys.* **1**(4), 264–280 (2019).
13. Q. Stahl, T. Ritschel, G. Garbarino, *et al.*, "Pressure-tuning of  $\alpha$ - $\text{RuCl}_3$  towards a quantum spin liquid," *Nat. Commun.* **15**(1), 8142 (2024).
14. Y. Kasahara, T. Ohnishi, Y. Mizukami, *et al.*, "Majorana quantization and half-integer thermal quantum hall effect in a Kitaev spin liquid," *Nature* **559**(7713), 227–231 (2018).
15. F. Bahrami, M. Abramchuk, O. Lebedev, *et al.*, "Metastable Kitaev Magnets," *Molecules* **27**(3), 871 (2022).
16. V. Hermann, M. Altmeyer, J. Ebad-Allah, *et al.*, "Competition between spin-orbit coupling, magnetism, and dimerization in the honeycomb iridates:  $\alpha$ - $\text{Li}_2\text{IrO}_3$  under pressure," *Phys. Rev. B* **97**(2), 020104 (2018).

17. K. Kitagawa, T. Takayama, Y. Matsumoto, *et al.*, “A spin–orbital-entangled quantum liquid on a honeycomb lattice,” *Nature* **554**(7692), 341–345 (2018).
18. K. Geirhos, P. Lunkenheimer, M. Blankenhorn, *et al.*, “Quantum paraelectricity in the Kitaev quantum spin liquid candidates  $\text{H}_3\text{LiIr}_2\text{O}_6$  and  $\text{D}_3\text{LiIr}_2\text{O}_6$ ,” *Phys. Rev. B* **101**(18), 184410 (2020).
19. S. Pei, L.-L. Huang, G. Li, *et al.*, “Magnetic Raman continuum in single-crystalline  $\text{H}_3\text{LiIr}_2\text{O}_6$ ,” *Phys. Rev. B* **101**(20), 201101 (2020).
20. A. de la Torre, B. Zager, F. Bahrami, *et al.*, “Momentum-independent magnetic excitation continuum in the honeycomb iridate  $\text{H}_3\text{LiIr}_2\text{O}_6$ ,” *Nat. Commun.* **14**(1), 5018 (2023).
21. T. Halloran, Y. Wang, K. W. Plumb, *et al.*, “Continuum of magnetic excitations in the Kitaev honeycomb iridate  $\text{D}_3\text{LiIr}_2\text{O}_6$ ,” *npj Quantum Mater.* **10**, 35 (2024).
22. S. Bette, T. Takayama, K. Kitagawa, *et al.*, “Solution of the heavily stacking faulted crystal structure of the honeycomb iridate  $\text{H}_3\text{LiIr}_2\text{O}_6$ ,” *Dalton Trans.* **46**(44), 15216–15227 (2017).
23. Y. X. Yang, C. Y. Jiang, L. L. Huang, *et al.*, “Muon spin relaxation study of spin dynamics on a Kitaev honeycomb material  $\text{H}_3\text{LiIr}_2\text{O}_6$ ,” *npj Quantum Materials* **9**, 77 (2024).
24. J. Knolle, R. Moessner, and N. B. Perkins, “Bond-Disordered Spin Liquid and the Honeycomb Iridate  $\text{H}_3\text{LiIr}_2\text{O}_6$ : Abundant Low-Energy Density of States from Random Majorana Hopping,” *Phys. Rev. Lett.* **122**(4), 047202 (2019).
25. A. de la Torre, D. M. Kennes, M. Claassen, *et al.*, “Colloquium: Nonthermal pathways to ultrafast control in quantum materials,” *Rev. Mod. Phys.* **93**(4), 041002 (2021).
26. J. H. Mentink, K. Balzer, and M. Eckstein, “Ultrafast and reversible control of the exchange interaction in Mott insulators,” *Nat. Commun.* **6**(1), 6708 (2015).
27. M. Claassen, H.-C. Jiang, B. Moritz, *et al.*, “Dynamical time-reversal symmetry breaking and photo-induced chiral spin liquids in frustrated Mott insulators,” *Nat. Commun.* **8**(1), 1192 (2017).
28. S. Kitamura, T. Oka, and H. Aoki, “Probing and controlling spin chirality in Mott insulators by circularly polarized laser,” *Phys. Rev. B* **96**(1), 014406 (2017).
29. D. M. Kennes, A. de la Torre, A. Ron, *et al.*, “Floquet engineering in quantum chains,” *Phys. Rev. Lett.* **120**(12), 127601 (2018).
30. N. Walldorf, D. M. Kennes, J. Paaske, *et al.*, “The antiferromagnetic phase of the Floquet-driven Hubbard model,” *Phys. Rev. Lett.* **100**(12), 121110 (2019).
31. T. Oka and S. Kitamura, “Floquet engineering of quantum materials,” *Annu. Rev. Condens. Matter Phys.* **10**(1), 387–408 (2019).
32. N. Arakawa and K. Yonemitsu, “Floquet engineering of Mott insulators with strong spin-orbit coupling,” *Phys. Rev. Lett.* **103**(10), L100408 (2021).
33. A. Sriram and M. Claassen, “Light-induced control of magnetic phases in Kitaev quantum magnets,” *Phys. Rev. Res.* **4**(3), L032036 (2022).
34. U. Kumar, S. Banerjee, and S.-Z. Lin, “Floquet engineering of Kitaev quantum magnets,” *Commun. Phys.* **5**(1), 157 (2022).
35. N. Tancogne-Dejean, M. A. Sentef, and A. Rubio, “Ultrafast modification of Hubbard  $U$  in a strongly correlated material: Ab initio high-harmonic generation in  $\text{NiO}$ ,” *Phys. Rev. Lett.* **121**(9), 097402 (2018).
36. D. R. Baykusheva, H. Jang, A. A. Husain, *et al.*, “Ultrafast renormalization of the on-site Coulomb repulsion in a cuprate superconductor,” *Phys. Rev. X* **12**(1), 011013 (2022).
37. O. Grånäs, I. Vaskivskiy, X. Wang, *et al.*, “Ultrafast modification of the electronic structure of a correlated insulator,” *Phys. Rev. Res.* **4**(3), L032030 (2022).
38. J. G. Rau, E. K.-H. Lee, and H.-Y. Kee, “Generic spin model for the honeycomb iridates beyond the Kitaev limit,” *Phys. Rev. Lett.* **112**(7), 077204 (2014).
39. M. P. M. Dean, Y. Cao, X. Liu, *et al.*, “Ultrafast energy- and momentum-resolved dynamics of magnetic correlations in the photo-doped Mott insulator  $\text{Sr}_2\text{IrO}_4$ ,” *Nat. Mater.* **15**(6), 601–605 (2016).
40. D. G. Mazzone, D. Meyers, Y. Cao, *et al.*, “Laser-induced transient magnons in  $\text{Sr}_3\text{Ir}_2\text{O}_7$  throughout the Brillouin zone,” *Proc. Natl. Acad. Sci.* **118**(22), e2103696118 (2021).
41. H.-Y. Chen, R. B. Versteeg, R. Mankowsky, *et al.*, “A setup for hard X-ray time-resolved resonant inelastic X-ray scattering at Swissfel,” *Struct. Dyn.* **11**(2), 024308 (2024).
42. F. Freund, S. C. Williams, R. D. Johnson, *et al.*, “Single crystal growth from separated educts and its application to lithium transition-metal oxides,” *Sci. Rep.* **6**(1), 35362 (2016).
43. Y. Cao, D. G. Mazzone, D. Meyers, *et al.*, “Ultrafast dynamics of spin and orbital correlations in quantum materials: an energy- and momentum-resolved perspective,” *Phil. Trans. R. Soc. A* **377**(2145), 20170480 (2019).
44. M. Mitrano and Y. Wang, “Probing light-driven quantum materials with ultrafast resonant inelastic x-ray scattering,” *Commun. Phys.* **3**(1), 184 (2020).
45. Y. Wang, Y. Chen, C. Jia, *et al.*, “Time-resolved resonant inelastic x-ray scattering in a pumped mott insulator,” *Phys. Rev. Lett.* **101**(16), 165126 (2020).
46. J. Park, I. Eom, T.-H. Kang, *et al.*, “Design of a hard X-ray beamline and end-station for pump and probe experiments at Pohang Accelerator Laboratory X-ray Free Electron Laser facility,” *Nucl. Instrum. Methods Phys. Res., Sect. A* **810**, 74–79 (2016).
47. I. Nam, C.-K. Min, B. Oh, *et al.*, “High-brightness self-seeded X-ray free-electron laser covering the 3.5 keV to 14.6 keV range,” *Nat. Photonics* **15**(6), 435–441 (2021).

48. C.-K. Min, I. Nam, H. Yang, *et al.*, “Hard X-ray self-seeding commissioning at PAL-XFEL,” *J. Synchrotron Radiat.* **26**(4), 1101–1109 (2019).
49. J. Lee, C. Hyun Shim, M. Yoon, *et al.*, “Optimization of the hard x-ray self-seeding layout of the PAL-XFEL,” *Nucl. Instrum. Methods Phys. Res., Sect. A* **798**, 162–166 (2015).
50. T.-K. Choi, J. Park, G. Kim, *et al.*, “Resonant X-ray emission spectroscopy using self-seeded hard X-ray pulses at PAL-XFEL,” *J. Synchrotron Radiat.* **30**(6), 1038–1047 (2023).
51. H.-S. Kang, C.-K. Min, H. Heo, *et al.*, “Hard X-ray free-electron laser with femtosecond-scale timing jitter,” *Nat. Photonics* **11**(11), 708–713 (2017).
52. L. Dai, J. Ye, and N. C. Greenham, “Thermalization and relaxation mediated by phonon management in tin-lead perovskites,” *Light: Sci. Appl.* **12**(1), 208 (2023).
53. V. Rizzi, T. N. Todorov, J. J. Kohanoff, *et al.*, “Electron-phonon thermalization in a scalable method for real-time quantum dynamics,” *Phys. Rev. Lett.* **93**(2), 024306 (2016).
54. S. Ono, “Thermalization in simple metals: Role of electron-phonon and phonon-phonon scattering,” *Phys. Rev. Lett.* **97**(5), 054310 (2018).
55. M. Eckstein, M. Kollar, and P. Werner, “Thermalization after an interaction quench in the Hubbard model,” *Phys. Rev. Lett.* **103**(5), 056403 (2009).
56. M. Eckstein and P. Werner, “Thermalization of a pump-excited Mott insulator,” *Phys. Rev. Lett.* **84**(3), 035122 (2011).
57. Y. Li, S. M. Winter, and R. Valentí, “Role of hydrogen in the spin-orbital-entangled quantum liquid candidate  $\text{H}_3\text{LiIr}_2\text{O}_6$ ,” *Phys. Rev. Lett.* **121**(24), 247202 (2018).
58. K. Foyevtsova, H. O. Jeschke, I. I. Mazin, *et al.*, “Ab initio analysis of the tight-binding parameters and magnetic interactions in  $\text{Na}_2\text{IrO}_3$ ,” *Phys. Rev. Lett.* **88**(3), 035107 (2013).
59. S. M. Winter, Y. Li, H. O. Jeschke, *et al.*, “Challenges in design of Kitaev materials: Magnetic interactions from competing energy scales,” *Phys. Rev. Lett.* **93**(21), 214431 (2016).
60. M. Merboldt, M. Schüler, D. Schmitt, *et al.*, “Observation of Floquet states in graphene,” (2024).
61. D. Choi, M. Mogi, U. D. Giovannini, *et al.*, “Direct observation of Floquet-Bloch states in monolayer graphene,” *arXiv* (2024).
62. J.-Y. Shan, M. Ye, H. Chu, *et al.*, “Giant modulation of optical nonlinearity by Floquet engineering,” *Nature* **600**(7888), 235–239 (2021).
63. A. de la Torre, B. Zager, F. Bahrami, *et al.*, “Enhanced hybridization in the electronic ground state of the intercalated honeycomb iridate  $\text{Ag}_3\text{LiIr}_2\text{O}_6$ ,” *Phys. Rev. Lett.* **104**(10), L100416 (2021).
64. J. H. Hubbell, “Tables of x-ray mass attenuation coefficients and mass energy-absorption coefficients,” <http://physics.nist.gov/PhysRefData/XrayMassCoef/> (1996).
65. M. Jenderka, R. Schmidt-Grund, M. Grundmann, *et al.*, “Electronic excitations and structure of  $\text{Li}_2\text{IrO}_3$  thin films grown on  $\text{ZrO}_2\text{:y}$  (001) substrates,” *J. Appl. Phys.* **117**(2), 025304 (2015).
66. E. Dufault, F. Bahrami, A. Streeter, *et al.*, “Introducing the monoclinic polymorph of the honeycomb magnet  $\text{Na}_2\text{Co}_2\text{TeO}_6$ ,” *Phys. Rev. Lett.* **108**(6), 064405 (2023).